VALIDATION REPORT

Fire Radiative Power

Product: FRP_Pixel (LSA-502) and FRP_Grid (LSA-503)

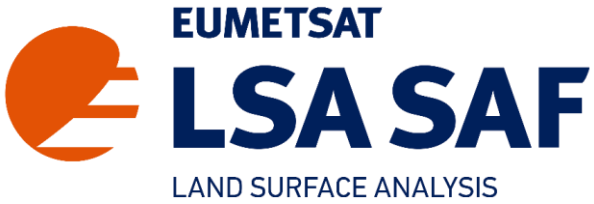

Reference Number:	SAF/LAND/IM/VR_FRP/2.0
Issue/Revision Index:	Issue 1
Last Change:	11/11/2015

DOCUMENT SIGNATURE TABLE

	Name	Date	Signature
Prepared by:	Land SAF Project Team		
Approved by:	Land SAF Project Manager (IPMA)		

DOCUMENTATION CHANGE RECORD

Issue / Revision	Date	Release	Description:
Version I/2008	25/03/2008	0.8	Version to be presented to ORR3
Version II/2008	20/05/2008	0.9	Version containing the modifications requested by ORR3.
Version III/2009	20/06/2009	1.1	Version containing the modifications requested by ORR3 and additional validation of FRP Pixel v1.1 product
Version IV/2009	14/09/2009	1.3	Version referring to the FRP Pixel v1.3 product
Version V/2009	18/10/2009	1.4	Version incorporating updates to FRP_Grid 0.4
Version VI/2010	19/03/2010	1.4	Version containing the modifications requested by LSA 32 FRP Grid ORR.
Version VII/2015	19/09/2015	2.0	Version containing the change of program language from C to Python, and the processing based on full disk instead of 4 regions. The content of the previous VR report can be found in the publications referred to herein (Wooster *et al.* (2015) and Roberts *et al.* (2015).

Table of Contents

Executive Summary 5

1. Introduction 7
- **1.1. Landscape Fire Observations with Meteosat 2nd Generation** 7
- **1.2. LSA SAF Meteosat SEVIRI FRP Products** 10
- **1.3 Definition of Accuracy Requirements** 15

2. Validation Datasets and Methods 16
- **2.1 FRP-PIXEL Product** 16
- **2.2 FRP-GRID Product** 19

3. Validation Results 20
- **3.1 FRP-PIXEL Product** 20
- **3.2 FRP-GRID Product** 27

4. Conclusions 29

List of Acronyms

ATBD	Algorithm Theoretical Basis Document
CASA	Carnegie-Ames-Stanford Approach
CPTEC	Centro de Previsão de Tempo e Estudos Climáticos
ECMWF	European Centre for Medium-range Weather Forecasts
EUMETSAT	European Organisation for Exploitation of Meteorological Satellites
FAS	Fire Assimilation System (at FMI)
FIR	Finitive impulse response
FMI	Finnish Meteorological Institute
HRV	High Resolution Visible
FRE	Fire Radiative Energy
FREEVAL	Fire Radiative Energy Evaluation
FRP	Fire Radiative Power
FTA	Fire Thermal Anomaly
GAS	GMES Atmospheric Service
GFED	Global Fire Emissions Database (GFED) (van der Werf *et al.* 2006)
IFS	Integrated Forecast System
INPE	Instituto Nacional de Pesquisas Espaciais
KCL	King's College London
NRT	Near Real Time
MACC	Monitoring of Atmospheric Composition and Climate
MIR	Middle InfraRed
MODIS	Moderate Resolution Imaging Spectroradiometer
MOPITT	Measurements of Pollution in the Troposphere
MPEF	Meteorological Product Extraction Facility at EUMETSAT
NOAA	National Oceanic and Atmospheric Administration
ORR	Operation Readiness Review
PM	Particulate Matter
RAO	Research Annoncement of Opportunity
SAF	Satellite Applications Facility
SEVIRI	Spinning Enhanced Visible and InfraRed Imager
TA	Thermal Anomaly [K]
TIR	Thermal InfraRed

Executive Summary

A series of active fire (AF) detection/fire radiaitve power (FRP) products are generated at the Land Surface Analysis Satellite Applications Facility (LSA SAF). The FRP-PIXEL (LSA-502) and FRP-GRID (LSA-503) products are derived using data from SEVIRI, which operates on-board the Meteosat Second Generation (MSG) series of geostationary EO satellites. The processing chain developed to deliver these FRP products detects SEVIRI pixels containing actively burning fires and characterises their FRP output across Europe, part of South America and Africa. The FRP-PIXEL product contains the highest spatial and temporal resolution FRP dataset, whilst the FRP-GRID product contains a spatio-temporal summary that includes bias adjustments for the non-detection of low FRP fire pixels and correction for cloud cover. Here we perform an evaluation of these two products, primarily using active fire detections and FRP data collected by the 1 km spatial resolution Moderate Resolution Imaging Spectroradiometer (MODIS). MODIS is generally accepted at the current standard for these types of products, and is able to detect fires of significantly lower FRP than SEVIRI due to its much higher spatial resolution. Data from July 2015 have been used herein, including FRP-PIXEL, FRP-GRID and AQUA/TERRA MODIS AF products. Results show that FRP measures included in FRP-PIXEL meet the product Target Accuracy, with 79% of the per-fire FRP measures within 50% of the FRP measured at the same fire near-simultaneosly with MODIS, and with the FRP-GRID data having 54% of the values within a facor of 2 of the equivalent value estimated using MODIS. In summary both the FRP-PIXEL and FRP-GRID products fulfil their Target Accuracy requirements, and are the highest temporal resolution FRP products currently available from Earth orbit. They therefore provide unique data for use in monitoring fire and smoke emissions from highly variable landscape combustion, including for use in atmospheric modelling aiming to elucidate fire emissions transport and downsteam effects.

Applicable Documents

[AD 1] The EUMETSAT Satellite Applications Facility on Land Surface Analysis Product Requirements Document, v2.8 July 2015

Reference Documents

[RD 1] The EUMETSAT Satellite Applications Facility on Land Surface Analysis Product User Manual for Fire Radiative Power Products, v2.0, November 2015

[RD 2] The EUMETSAT Satellite Applications Facility on Land Surface Analysis ATBD of for Fire Radiative Power Products, v2.8, November 2015

1. Introduction

1.1. Landscape Fire Observations with Meteosat 2nd Generation

The European Organisation for the Exploitation of Meteorological Satellites (EUMETSAT) currently operates the Meteosat Second Generation (MSG) system, Europe's geostationary Earth Observation (EO) programme for studying weather, climate and the environment. Since the first MSG launch in 2002, the Spinning Enhanced Visible and Infrared Imager (SEVIRI) has provided multispectral, radiometrically calibrated data of Europe, Africa, and a part of South America every 15 minutes at a 3 km spatial sampling distance (more as you get further away from the sub-satellite point; SSP). SEVIRI data is capable of being used to detect actively burning fires (Figure 1a) and the Fire Radiative Power (FRP) of the detected fires can be estimated from the recorded IR radiances. FRP has been shown to be directly related to rates of fuel consumption and smoke production (e.g. Freeborn *et al.* 2008; Kremens *et al.* 2012; Pereira *et al.* 2011; Wooster *et al.* 2005), and SEVIRI in fact provided the first geostationary EO data to be used to estimate FRP from landscape-scale vegetation fires (Roberts *et al.* 2005; Roberts and Wooster 2008; Wooster *et al.* 2005). SEVIRI FRP data are generated at the LSA SAF in near real time in two product forms (full resolution FRP-PIXEL and and hourly summary product FRP-GRID) and are now being used to paremeterise high temporal smoke emissions fields for use in atmospheric modelling (e.g. Baldassarre *et al.*, 2014), including in the models used within the prototype GMES/Copernicus Atmosphere System (Roberts *et al.*, 2015). The direct near-real time retrieval of FRP almost continueously from geostationary orbit provides a unique view of combustion whilst fires are still burning.

This validation report focuses on demonstrating the extent to which the LSA SAF FRP-PIXEL and FRP-GRID products meet their accuracy requirements, and providing an overview of overall product performance. The prior version of this validation report contained additional information on product algorithm stages, impacts of the SEVIRI level 1.0 to 1.5 pre-processing chain, and a demonstration of use within atmospheric models. This information can now be variously found in the product Algorithm Theoretical Basis Document (Govaerts *et al.*, 2015) and Product User Manual (EUMETSAT, 2015), listed as Reference Documents above, and in two papers (Wooster *et al.*, 2015 and Roberts *et al.*, 2015) detailed in the Reference List.

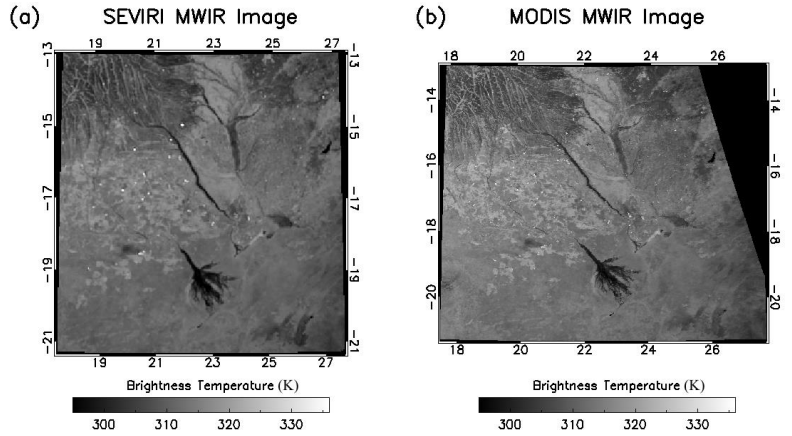

Figure 1. Near simultaneous MWIR imagery of fires in southern Africa from (a) SEVIRI (IR3.9) and (b) MODIS (Band 21), showing pixels with elevated MWIR brightness temperatures as bright, and almost all of these are likely fires. The area shown includes the Okavango delta wetland (around 250 km long) and were collected at 12:50 UTC on 17th August 2007 (10 mins time difference between MODIS and SEVIRI). The polar orbiting MODIS and geostationary SEVIRI data are not exactly co-registered, but cover approximately the same area. Whilst the increased spatial resolution of the MODIS data is clear, and allows more fires to be visually identified via their elevated MWIR signals, many of the fires can also clearly be seen in the SEVIRI imagery (albeit with lower MWIR brightness temperatures since each fires will be filling a lower proportion of the larger SEVIRI pixel than the smaller matching MODIS pixels). SEVIRI provides 96 images per day at a consistent view zenith angle, whilst at this latitude MODIS provides up to four images per day, though some will be at extreme view zenith angles up to 65° where the MODIS spatial fidelity is far reduced and MODIS pixels cover approximately the same ground area as does a nadir SEVIRI pixel. The local afternoon imaging time of MODIS Aqua used here is relatively close to the typical peak of the fire diurnal cycle, but the times of the other MODIS overpasses are significantly distant from this.

Whilst MSG proves to have an excellent capabilty to active fire osbervations, it is not perfect and some characteristics limit the precision of the resulting FRP data. Saturation occurs in the SEVIRI IR3.9 channel at a MWIR brightness temperature of 335 K, and high FRP fires can this saturate the imager in this channel. Saturated fire pixels in the FRP products have their FRP upwardly adjusted to account for certain of the biases involved and thus estiamte the true FRP (albeit with larger uncertainties than for non-saturated fire pixels), and are flagged as FRP derived from a saturated pixel in the FRP products (specifically the FRP-PIXEL Quality Product discussed

herein). Full details of this and all other key product characteristics are included in the FRP Product Product User Manual (PUM) available at the LSA SAF website ((http://landsaf.ipma.pt), and in Wooster *et al.* (2015). There are also certain imaging artefacts present in the SEVIRI data of active fires, that impact for example the IR3.9 brightness temperatures seen surrounding active fire pixels (demonstrated in Figure 2). To deliver the anti-aliased properties specified for SEVIRI level 1.5 imagery (Just, 2000; Deneke and Roebeling 2010), a Finite Impulse Response (FIR) digital filter is applied to each line of SEVIRI data and it is this filter which leads to the BT peterbations seen in Figure 2 (Wooster *et al.*, 2015). All these effects are planned to be removed in the Meteosat Third Generation system, but currently impact the precision of the MSG SEVIRI FRP retrievals. This contributes both to the FRP uncertainty estimates provided in the FRP product delivered by SEVIRI, and to differences seen beteween MODIS and SEVIRI FRP measures seen simultaneously at the same fires as assessed in this report. Users should be aware that beyond a SEVIRI view zenith angle of around 60° (i.e. towards the edge of the SEVIRI disk) the FRP product performance degrades substantially due to the extreme pixel sizes and view angles involved, and thus users may wish to discard data outside of this view angle limit. Further information on this is detailed in the FRP Product Product User Manual (PUM).

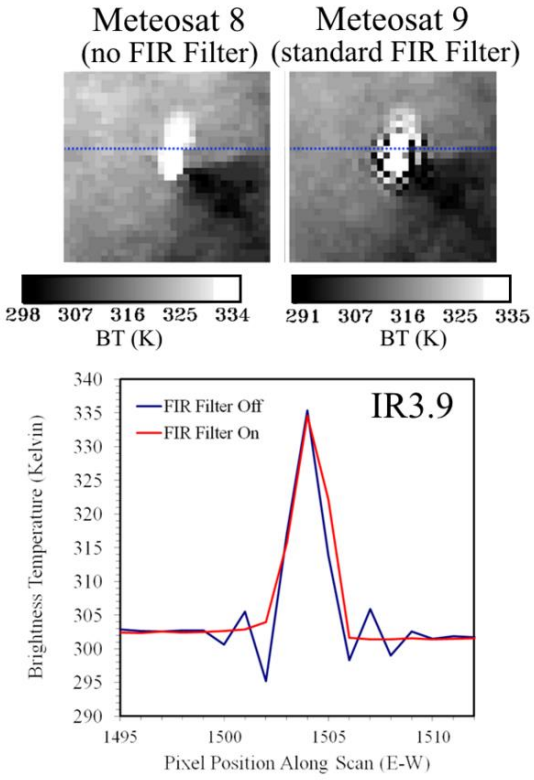

Figure 2: Near simultaneous Meteosat-8 and -9 Band 4 (MWIR) Imagery of a large, intensely burning (high FRP) fire in southern Africa taken on 3 September 2007 during a period of Meteosat-8 'Special operations' when the satellite had the application of certain pre-processing digital filters removed temporarily. Data appear somwhat different to that collected with the normally operating Meteosat-9, as expained in Wooster *et al.* (2015), particularly the brightness temperature peturbations seein the in Meteosat-9 data either side of the fire pixels.

1.2. LSA SAF Meteosat SEVIRI FRP Products

Two operational SEVIRI FRP products are delivered from Meteosat Second Generation in near real-time and archived form by the LSA SAF, whose role is to take full advantage of remotely sensed data to support land, land–atmosphere and

biosphere applications, with an emphasis on the development and implementation of algorithms allowing operational use of EUMETSAT satellites (Trigo *et al.*, 2011).

The primary LSA SAF Meteosat SEVIRI FRP output is the Level 2 FRP-PIXEL product, delivered at the full spatial and temporal resolution of SEVIRI covering Europe, Africa and part of South America, and a secondary output is a Level 3 spatio-temporal summary of these termed the FRP-GRID product.

The FRP-PIXEL product provides information on the spatial location, thermal properties, atmospherically corrected FRP and uncertainty of pixels containing actively burning fires every 15 minutes, based upon an extended version of the geostationary Fire Thermal Anomaly (FTA) active fire detection algorithm of Roberts and Wooster (2008), along with a set of FRP estimation routines that are together fully detailed in Wooster *et al.* (2015). The FRP-PIXEL product is delivered in two separate fires, a List Product file where the FRP records of all detected active fire pixels are provided, and a Quality Product where each pixel in the Meteosat disk is given a class related to whether or not it contains a fire, and if not why not. as fully explained in the FRP Product User Manual (PUM) already referred to.

From the FRP-PIXEL List Product, Figure shows the mean FRP of each SEVIRI pixel identified as a fire over seven years from 2008 to 2013. The data show that the major fire affected areas are southern Africa, Central Africa and South America. Curently areas of the SEVIRI disk are delivered in separate output files, but a single full disk product will replace the four geographical regions in the new product version to be delivered from late 2015, as explained in the LSA SAF FRP Product User Manual (PUM) already referred to.

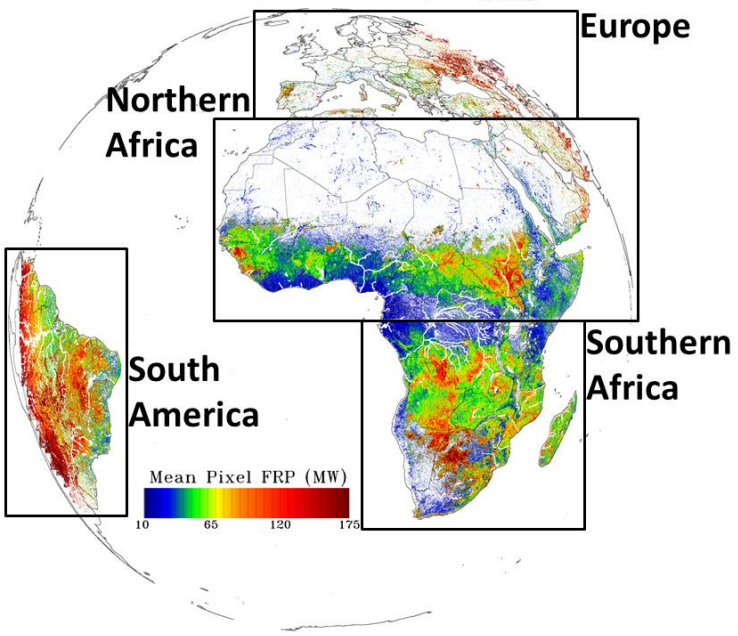

Figure 3. SEVIRI's imaging disk showing the mean per-pixel FRP (MW) seen in each SEVIRI pixel, calculated using all FRP-PIXEL products from 2008 to 2013. Also notices the four geographic regions that LSA-SAF SEVIRI products definded in previous version will be combined into one full disk product.

Figure shows an example of full disk quality product recorded at 13:00 UTC on 10th July 2015. Confirmed fire pixels are shown in red, cloud in white and fire-free land pale brown. All FRP product files are stored in HDF5 format, and further details on their contents and accessibility can be found in Wooster *et al.* (2015) and the FRP Product User Manual (PUM).

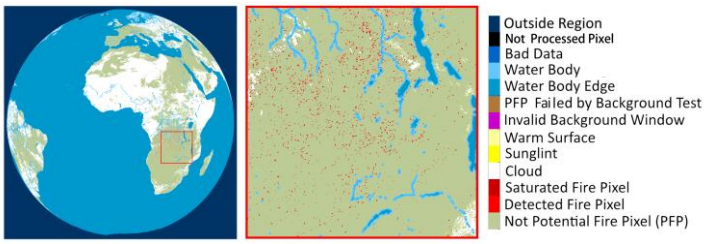

Figure 4. FRP-PIXEL quality product classification scheme applied to the Meteosat full disk data taken at 13:00 UTC on 5th July 2015. The figure on the left show full disk, the middle figure is a zoomed in versions in full disk over Southern Africa where the majoyority of fires occurred. The panel on right shows the classification names. Full details of the product can be found in Wooster *et al.* (2015) and a colour paleltte has been applied here to display the data most effectively.

The secondary LSA SAF Meteosat SEVIRI FRP output is a Level 3 spatio-temporal summary of a series of FRP-PIXEL products, termed the FRP-GRID product. This is issued hourly at a 5-degree grid cell size, and Figure 5 shows an example of the FRP recorded in the FRP-GRID Product.

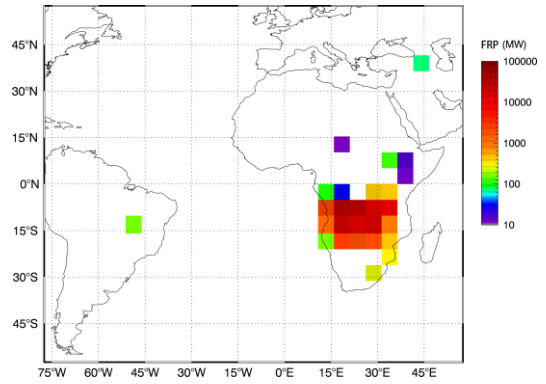

Figure 5. Example of FRP-GRID product recoded on 5 July 2015, 12:00 UTC. The total per-slot FRP recorded from fires detected in each 5-degree grid cell is reported, given as the mean FRP detected in the cell over the last hour. Fires are here primarily located in southern Africa.

Whilst the very high temporal resolution of the input SEVIRI dataset allows the FRP-PIXEL product to provide an unprecedentied temporal insight into the changing combustion regime of the observed regions, and for example otherwise unobtainable information on details of the fire dirunal cycle (Roberts *et al.*, 2009), it does have some limitations in terms of the type of fire fire activity that is able to be quantified. In particular, the FRP-PIXEL product provides a minimum estimate of the FRP being emitted from landscape fires because of (i) the inability of the relatively courase spatial resolution SEVIRI data to detect the lowest FRP active fire pixels (Roberts and Wooster, 2008; Freeborn *et al.*, 2014a) and (ii) the fact that the assessment of the highest FRP fires suffer from some adverse effects related to pixel saturation and other SEVIRI-specific observation characteristics as discussed above and in further detail in Wooster *et al.* (2015). In order to mitigate these impacts on regional FRP estimation, the Level 3 FRP-GRID product includes certain bias adjustement factors,

which are applied to the temporally accumulated active fire pixels (and associated information) held within the maximum of four FRP-PIXEL products obtained across the full disk each hour. Wooster *et al.* (2015) and the LSA SAF FRP Product User Manual (PUM) describe the FRP-GRID prodct in full, and Freeborn *et al.* (2009) describe certain of the ideas behind the bias-adjustement procedures applied.

The purpose of this Validation Report is to provide information regarding the evaluation of these two FRP products: FRP-PIXEL and FRP-GRID. The evaluation is based upon comparisons to active fire data collected by the polar orbiting MODIS instrument. The relatively high spatial resolution of MODIS' active fire observations (1 km at nadir), and the high saturation temperature of its MIR channel (~ 500 K), coupled with its better than daily availability from two platforms (the Terra and Aqua satellites), ensure that the MODIS active fire detection and FRP product (Kaufman *et al.*, 1998; Giglio *et al.* 2003) are the standard against which geostationary active fire products are compared when performing product evaluations (e.g. Xu *et al.*, 2010; Schroeder *et al.*, 2014; Roberts and Wooster *et al.*, 2015). Here we use near-simultaneously recorded Collection 5 MODIS active fire detections (MOD14 from Terra and MYD14 from Aqua) as the basis of our LSA SAF SEVIRI FRP Product performance evaluation.

1.3 Definition of Accuracy Requirements

The user requirements for FRP products in general were collected in Table 1 below. Here, we assess the accuracy requirements specifically for the SEVIRI FRP product and in light of the theoretical performance that is achievable with this sensor under its standard operating conditions.

The three accuracy values tabulated below are defined as follows:

- *Threshold accuracy:* this is the accuracy limit, which is needed so that the product fulfils its purpose.
- *Target accuracy:* this is the average product accuracy under the present operating conditions and with the instrument characteristics of SEVIRI. With this product quality the product will be valuable for most of the users identified above.
- *Optimal accuracy:* this is the accuracy that can be reached under optimum conditions (sub-satellite point, cloud-free scene, homogeneous background, medium sized fire).

The accuracy of the SEVIRI FRP product will depend on various factors related to pixel resolution, channel saturation, viewing geometry and on-board and ground-based pre-processing of raw signals (Wooster *et al.*, 2015). Furthermore, the required level of accuracy will depend on the application, and different aspects of accuracy might be emphasized in different applications. For example, a fire warning system will be less concerned about the absolute quantitative value of FRP as long as the fire can be reliably detected rapidly (with as few commission errors in particular) and there is some indication about fire severity. Atmospheric chemistry forecasts, and even more so reanalysis simulations, on the other hand, depend on the reliability of area-averaged fire emissions (and thus FRP) and have less concern about the ability of the instrument to capture each and every fire.

Table 1: Summary of accuracy requirements for FRP-Pixel and FRP-GRID products.

Product	Threshold	Target	Optimal
FRP-PIXEL (LSA-502)	successful detection of a significant fraction of fires reproducing the spatial and temporal distribution	70% of retrieved FRP within 50% of "true" values as defined by MODIS on a fire basis	70% of retrieved FRP within 20% of "true" values as defined by MODIS10% on a fire basis
FRP-GRID (LSA-503)	anything is useful as long as not biased: NAfr/SAfr: 20% of predictions within 100% of MODIS measurement of FRP SAme: 15% of predictions within 100% of MODIS measurement of FRP Euro: 5% of predictions within 100% of MODIS measurement of FRP	NAfr/sAfr: 50% of predictions within 100% of MODIS measurement of FRP SAme/Euro: 25% of predictions within 100% of MODIS measurement of FRP	50% of predictions within 30% of MODIS measurement of FRP

[1] successful detection of a significant fraction of fires reproducing the spatial and temporal distribution can be considered the threshold target

2. Validation Datasets and Methods

2.1 FRP-PIXEL Product

The full disk FRP-PIXEL product generated by LSA SAF in July 2015 is used for this study, together with the matching MODIS MOD14 and MYD14 products. A total of 2843 FRP-PIXEL products and 567 MODIS products are used, along with 729 FRP-GRID files. Freeborn *et al.* (2014) found that FRP-PIXEL active fire detection errors of commission reduced greatly (from 24% to 9%) when the MODIS active fire detections being used as the independent data source for the evaluation were limited to a ± 18.6° scan angle. Therefore, to mitigate against the impact of MODIS' decreasing ability to detect low FRP pixels as MODIS scan angle increases, yet balance this with the need to maintain sufficient data in our intercomparison, we limited use of MODIS observations to those within ± 30° scan angle within which MODIS' pixel area increases up to a maximum of 1.7 km² from the nadir 1 km² size (Freeborn *et al.*, 2011).

We compared the active fire detections made by MODIS within the 30 degree scan angle limit to the active fire pixels present in the FRP-PIXEL product subsets covering the same area and collected at the closest matching time (generally this will be within ~ 6 minutes of the MODIS overpass). To deal with the differing MODIS and SEVIRI pixel sizes, we remapped the MODIS active fire data to SEVIRI's imaging grid. SEVIRI's per-pixel point spread function (PSF) at the sub-satellite point extends more than 5 km radially from the pixel centre (Wooster *et al.*, 2015), so following the approach of Freeborn *et al.* (2014) we evaluated active fire detection performance using the presence of an active fire pixel within a 3 × 3 pixel window centred on the active fire pixel under investigation within this grid as a matched detection. For SEVIRI errors of commission we searched for the presence of a matching MODIS pixel for each SEVIRI active fire pixel studied, whilst the reverse analysis was conducted for SEVIRI errors of omission.

Figure shows one scene pair of MODIS and SEVIRI data recorded at 12:00 UTC on 5th July 2015 over Southern Africa. Figure 6a shows the brightness temperature difference between the **SEVIRI** middle infrared **(IR3.9)** and **longwave** infrared **(IR10.8)** band**s**, one of the key metrics used in active fire detection (Roberts and Wooster, 2008; Wooster et al, 2015). The cloud and water bodies are masked out, with the active fire pixels as bright points in the **brightness temperature (BT)** difference figure. Figure b shows the active fires detected by MOIDS mapped into the SEVIRI projection (only those fires having a MODIS scan angle less than 30 degree are shown). Figure c illustrates the active fire detections from the FRP-PIXEL product made in the same area as the MODIS subscene. There are clearly many small fires missed by the FRP-PIXEL product, which MODIS does detect. This is mainly due to the much higher nadir spatial resolution of MOIDS (1 km), which is nearly three times the spatial sampling distance of SEVIRI (3 km) at the SEVIRI sub satellite point (SSP)**,** and around 4 km of the SEVIRI sampling distance in this region. Overall in this subscene, MODIS detected 2746 fire pixels, of which 912 (~33%) have a corresponding pixel in the FRP-PIXEL product. At the same time, **the** FRP-PIXEL **product** detected 1091 fire pixels, with 1005 (~92%) hav**ing** a corresponding MODIS **active** fire pixel. This demonstrates a good SEVIRI FRP-PIXEL active fire pixel detection rate when the spatial resolution difference between the two sensors is considered.

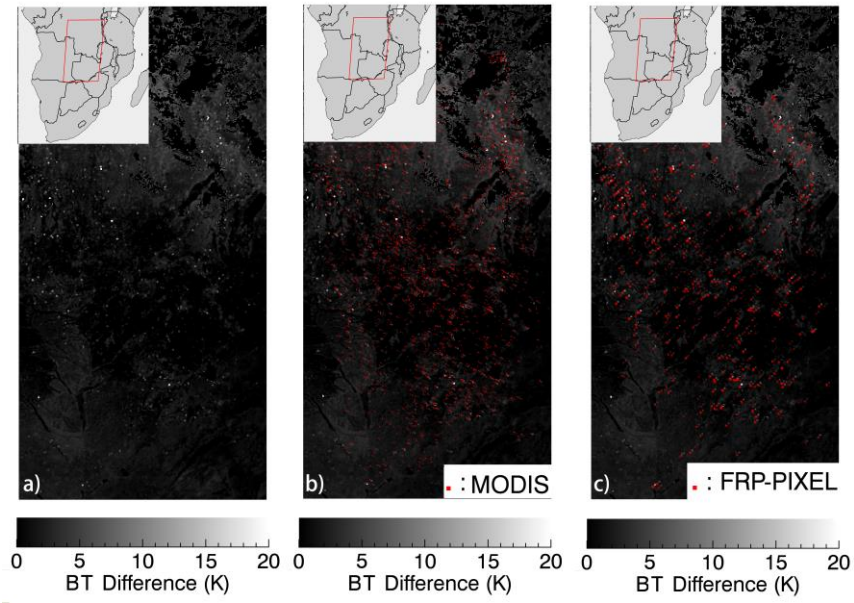

Figure 6. MODIS and FRP-PIXEL detected active fires overlain on a brightness temperature (BT) difference image (middle infrared - longwave infrared) taken by SEVIRI at 12:00 UTC on 5th July 2015 over Southern Africa. a). BT difference between middle infrared and thermal infrared; b). Fires detected by MODIS has a scan angle within 30 degree; c) Fires detected by FRP-PIXEL within the same MODIS scan area. In this scene, MODIS detected 2746 active fire pixels, and 912 fire pixels (~33%) among those have a corresponding pixel in the FRP-PIXEL product. At the same time, the FRP-PIXEL product detected 1091 active fire pixels, with 1005 (~92%) of those having a corresponding pixel in the MODIS dataset.

For the SEVIRI-to-MODIS FRP intercomparison, the FRP of each active fire pixel detected by MODIS was derived using the same MIR radiance approach to FRP derivation as is used for SEVIRI (Wooster *et al.*, 2005; 2015). This approach will also be employed in the forthcoming Collection 6 MODIS Active fire products (L. Giglio, *pers comm*.). We atmospherically corrected these MODIS FRP estimates using the same procedure applied when generating the FRP-PIXEL product, detailed in Wooster *et al.* (2015), based on an atmospheric transmission look-up-table (LUT) developed using the MODTRAN5 atmospheric radiative transfer models (Berk *et al.* 2005; Govaerts, 2006), ECMWF forecasts of total water column vapour (interpolated from an original spatial and temporal resolution of 0.5° and 3 hours), and information on the MODIS 3.9 μm channel spectral response. Generally, the adjustment for the

MWIR atmospheric transmission made to the SEVIRI FRP data was larger than that for MODIS, because the width of the SEVIRI IR3.9 spectral band is significantly wider than that of MODIS and extends into spectral regions having much lower atmospheric transmission than does the MODIS band (Wooster *et al.*, 2015).

2.2 FRP-GRID Product

We evaluated the performance of the bias adjustments applied during the FRP-GRID product generation using a validation dataset composed of coincident SEVIRI and MODIS observations, collected again in July 2015. The relevant fire pixels from MODIS that have a scan angle less than 30 degree were again used, and the boundaries encompassing these pixels were in this case used to identify 5° regions for the comparision. Active fire pixels detected by MODIS outside of this region of interest were not used during the analysis. Figure shows an example of one scene of MODIS data taken at 12:30 UTC on 10th July 2015. The red dots are the active fires from MODIS having a scan angle less than 30°. The two 5 × 5 degree grid cells bounded by the green borders are the only grid cells that are defined by, and covered in full, by those fires. Therefore only these two grid cells were used in the comparison on this particular SEVIRI-to-MODIS matchup. This sampling design ensured complete coverage of the 5.0° grid cells regardless of the MODIS ground track, and also mitigated the effects of image distortion at the edge of the MODIS swath. All MODIS granules collected during the study period were matched to the most concurrent FRP-GRID product, always within half hour of each other. Since FRP-GRID is the average of the previous hour of data (i.e. FRP-GRID at 13:00UTC is the average of 12:15, 12:30, 12:45 and 13:00 UTC of the corresponding FRP-PIXEL data) only MODIS data from 12:15 UTC to 12:45 UTC were used in the comparison (i.e. and mean time of 12:30 UTC that matches that of the FRP-GRID product).

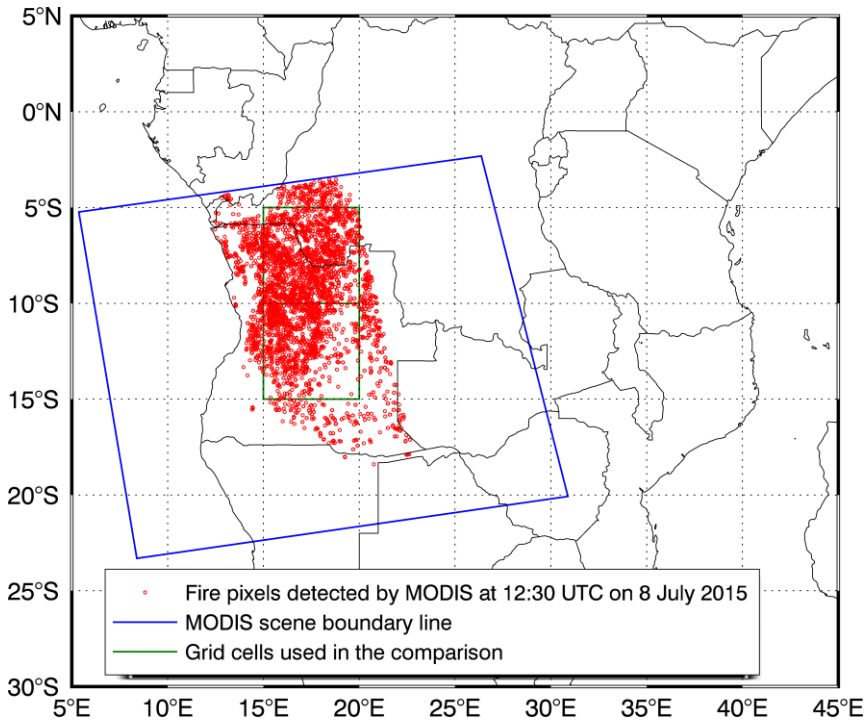

Figure 7. Active fires from MODIS detected at 12:30 UTC on 8th July 2015 over Southern Africa. The blue lines are boundary of full scene of MODIS, the red dots are those fires from MODIS having a scan angle < 30 degree. Two 5 × 5 degree grid cells with green boundaries lie towards the middle of MODIS swath, are well covered with fires, and are thus those used in the comparison from this particular MODIS-to-SEVIRI matchup.

3. Validation Results

3.1 FRP-PIXEL Product

3.1.1 Broad Dataset Characteristics

At total of 2843 FRP-PIXEL full disk products covering July 2015 were processed for this performance evaluation, and were compared against the active fire data recorded near simultaneously from MODIS. Figure 8 shows the fire diurnal cycle recorded by SEVIRI over the full disk during the month of July 2015 (local solar time: LST) for reference. Fire activity generally starts in the early morning, peaks around 13:00 LST and weakens in the afternoon. The diurnal cycle is key fire dynamic which can only

be revealed by geostationary satellites (Roberts *et al.*, 2005; Roberts and Wooster 2008). Geostationary data also typically maximise the number of cloud-free views of fire events, and allow the daily temporal integration of FRP to fire radiative energy and thus total fuel consumption and smoke emission (Roberts *et al.* 2009a; Roberts *et al.* 2009b). What is more, geostationary satellites often have a better opportunity to detect small fires in early stage, potentially giving better timeliness with regards to landscape management, response planning and fire suppression operations (Wooster *et al.* 2015; Xu *et al.* 2010).

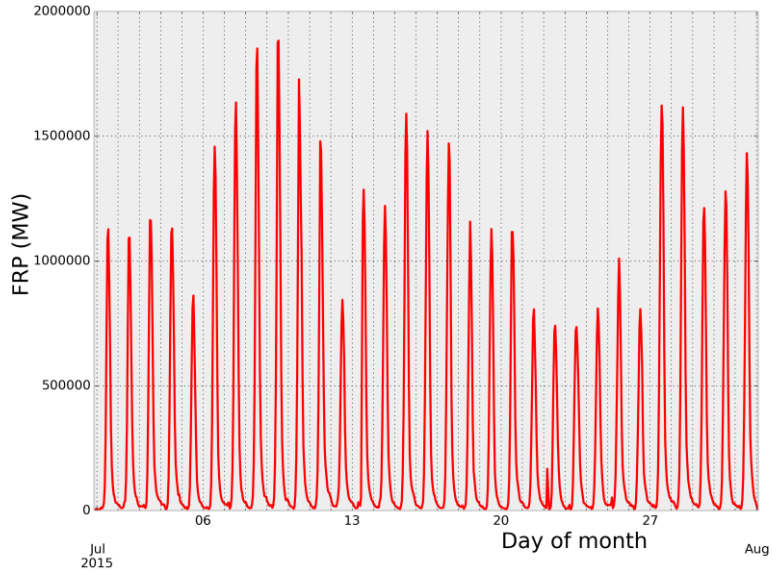

Figure 8. Fire durinal cycle seen across the full Meteosat disk as derived from FRP-PIXEL data recorded in July 2015 and plotted against local time of day (day of month shown). Fires peak in the early afternoon every day. Fire activity follows climate, and at this time of year most fire activity detected by SEVIRI is actually located in southern Africa rather than spread evenly across the disk.

3.1.2 Active Fire Errors of Omission and Commssion

The summary of results of the SEVIRI-to-MODIS per-pixel active fire detection intercomparison are detailed in Table 1. From the full disk analysis, we find that 71% of MODIS' active fire detections had no corresponding SEVIRI-detected active fire within the closest matching (in time) FRP-PIXEL product file. This 'active fire error

of omission' rate is close to that found by Roberts *et al.* (2015) over the southern Africa area, which is where most fires were located during the July 2015 period of the study dataset. The reverse analysis showed that 13% of the FRP-PIXEL product active fire pixels had no matching MODIS active fire pixel, a very similar active fire commission error to that found by Roberts *et al.* (2015) for the SEVIRI FTA algorithm over the southern African region. If we restrict our analysis area to southern Africa only, the active fire error of comission is reduced to 12%, and the error of ommission to 68%.

Table 2. SEVIRI FRP-PIXEL Product active fire detection errors in comparison to MODIS.

LSA SAF Geographic Region	Full Disk	Southern Africa
Number of SEVIRI FRP-PIXEL active fire pixels present at a coincident MODIS overpasses	53883	51912
Number of SEVIRI active fire pixels detected by MODIS	47035	45934
FRP-PIXEL Active Fire Detection Commission Error	13%	12%
FRP-PIXEL Active Fire Detection Omission Error	71%	68%

The per-pixel FRP frequency-density *vs.* FRP magnitude distribution of all coincident fires detected by FRP-PIXEL and those from the MODIS MOD14/MYD14 products were analysed for July 2015 and are shown in Figure 9. Between 30 MW and 220 MW the FRP-PIXEL and MODIS MOD14/MYD14 data show an excellent degree of agreement in terms of their frequency density-magnitude distributions, providing strong confidence in the SEVIRI active fire measurements.

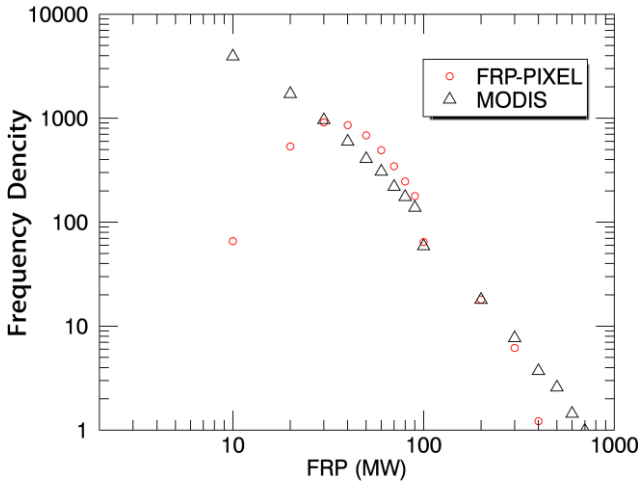

Figure 9. Frequency density *vs.* FRP magnitude distributions of MODIS and SEVIRI FRP-PIXEL data, constructed from coincident active fire pixels detected by SEVIRI and MODIS over the Southern African region in July 2015. The lower breakpoint of the SEVIRI distribution (around 30 MW) coincides with the decline in SEVIRI's active fire detection performance as the thermal radiance emitted from small and/or lower intensity fires cannot be reliably distinguished from that of the background window, and so many fires with an FRP below this limit remain undetected. The upper breakpoint (around 220 MW) coincides with the onset of SEVIIRI IR3.9 detector saturation. The FRP-GRID product aims to help account for the FRP that SEVIRI fails to detect as a result of these sensor artefacts, as well as by that due to cloud obscuration.

It is interesting to note that if the active fire detection algorithm of Giglio *et al.* (2003) (used to generate the Collection 5 MOD14/MYD14 MODIS active fire products) were applied to SEVIRI level 1.5 imagery, the minimum FRP detection limit at the Meteosat SSP would be around 70 - 80 MW, around 10× the minimum FRP detection limit of the MOD14/MYD14 active fire products due to SEVIRI's ~ 10× larger nadir view pixel area. However, the design of the FRP-PIXEL product attempts to lower the minimum FRP detection limit significantly below this by detecting active fire pixels whose radiometric signals in the MWIR, LWIR and MWIR-LWIR are raised even quite minimally above that of the ambient background (Roberts and Wooster, 2008). By exploiting a variety of spectral and spatial thresholds and contextual processing methods, the FTA algorithm is capable of reasonably confidently detecting SEVIRI active fire pixels having an FRP down to ~ 30 MW, as can be seen in Figure 9.

3.1.2 "Per fire" SEVIRI to MODIS Intercomparison

Figure presents the results of the SEVIRI-to-MODIS "per-fire" FRP intercomparison, where the FRP measures made by each sensor for the same fire at almost the same time are intercompared. On a per-fire basis there is a strong correlation (r^2 =0.74) between the FRP measures made by SEVIRI and by MODIS near simultaneosuly, and a slope of the linear best fit line close to unity (0.97). Overall, 79% of the SEVIRI-to-MODIS matchups have an FRP difference of less than 50%, and 62% of them less than 30%. 53% of the FRP-PIXEL products per-fire FRP measures are also within 20% of those of MODIS. The scatter present in the near-simultaneosly assessed MODIS and SEVIRI FRP maybe impacted by:

- Uncertainty in the ambient background signal used to calculate the FRP for each fire pixel with SEVIRI and MODIS data (Wooster *et al.*, 2003; 2005; Zhukov *et al.*, 2006; Wooster *et al.*, 2015);
- The max ± 6 minute time difference between corresponding MODIS and SEVIRI observations of the same fire, during which changes in the active fire characteristics that determine the fires FRP may occur;
- The significant uncertainties present in the MODIS FRP measures coming from the sub-pixel location of the fire with respect to the sensor instantaneous field of view, a factor recently characterised by Freeborn *et al.* (2014c). Also of significance are the SEVIRI measurement artifacts that are a result of the SEVIRI level 1.5 data production chain shown earlier in Figure 2 that can impact the uncertainty of the SEVIRI-based FRP retrievals (Wooster *et al.*, 2015). Freeborn *et al.* (2014c) suggest that MODIS FRP measures are uncertain to ± 30% due to the varying location of the active fires within the MODIS pixels, and a similar value is applicable to SEVIRI.
- Effects of saturation of SEVIRIs IR3.9µm channel at high FRP fire pixels.

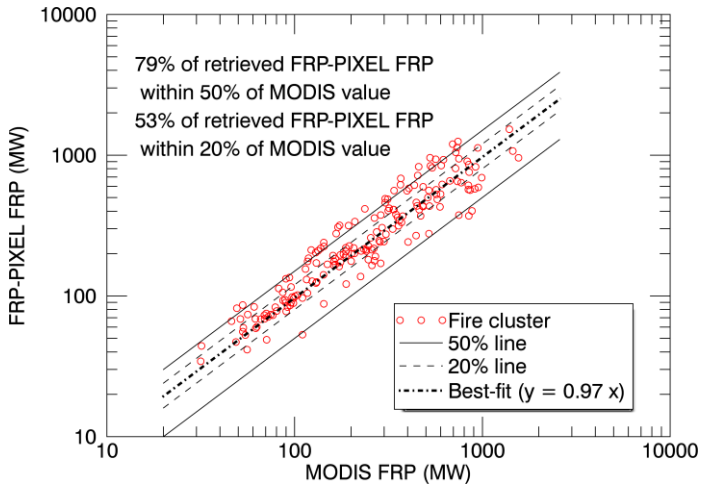

Figure 10. A comparison of FRPs measuremed at the same fires by the SEVIRI FRP-PIXEL and MODIS MOD15/MYD15 datasets in July 2015. Each circle represents a fire cluster, which is a contiguous or near-contiguous group of active fire pixels.

3.1.3 Regional Scale "FRP Areal Sum" Intercomparison

Whilst the above per-fire FRP inter-comparison has indicated a low degree of FRP bias between the FRP-PIXEL and MODIS MOD14/MYD14 FRP records of the same successfully detected active fires, there remains an expected and significant regional-scale FRP underestimation by the FRP-PIXEL product, due to its inability to detect the lowest FRP component of a regions fire regime (Roberts and Wooster, 2008), as already evidenced in the frequency-magnitude 30 MW breakpoint for SEVIRI shown in Figure 9. Therefore, when data from the MODIS MOD14/MYD14 products are compared to the near-simultaneous matching FRP-PIXEL products covering the same region (e.g. the area covered by a MODIS scene within a ±30° scan angle), the FRP-PIXEL product reports a lower cumulative 'regional' FRP than does MODIS as it will not detect many of the fires lower than 30 MW which MODIS can mainly detect. This effect is directly related to SEVIRI's active fire errors of omission, an effect magnified in geographic regions in which SEVIRI mostly observes at higher view zenith angles. Figure 11 uses the example of southern Africa, where the slope of the linear best fit to the regional FRP totals recorded near simultaneously in the FRP-PIXEL product and the MODIS active fire products is 0.79. Overall, 68% of the SEVIRI-to-MODIS regional scale matchups have an FRP difference less than 50%, 49% of them have an FRP difference of less than 30%, and 33% an FRP difference of less than 20%.

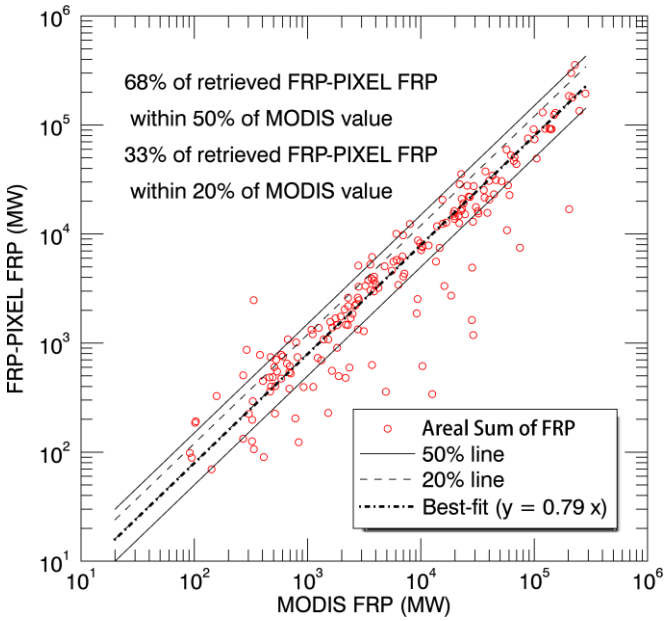

Figure 11. Relationship between regional-scale inter-scene FRP derived from all spatially matched, contemporaneous SEVIRI and MODIS in July 2015. The MODIS swath where fires have a scan angle less than 30 degree is taken as the observation area. The least squares linear best-fit passing through the origin is shown (dot dash line), along with the 50% and 20% line (solid and dash line). FRP-PIXEL tends to generally underestimate regional-scale FRP, primarily due to the non-detection of the lowest FRP fire pixels, many of which MODIS can detect. However, since the FRP of each of the undetected active fires is typically low, the degree of underestimation is relatively small compared to the active fire errors of omission. The FRP-GRID product is designed to in part adjust for this underestimation.

If only those fires detected by both SEVIRI and MODIS are included in the regional scale comparison shown in Figure 11, thus largely removing the "small fire" negative bias present in the SEVIRI data of Figure 12, then the slope of the linear best fit between SEVIRI and MODIS returns to very close to unity (1.07), as seen in Figure 12. Overall, 80% of the SEVIRI-to-MODIS matchups have an FRP difference less than 50%, 70% of them less than 30%, and 59% less than 20%.

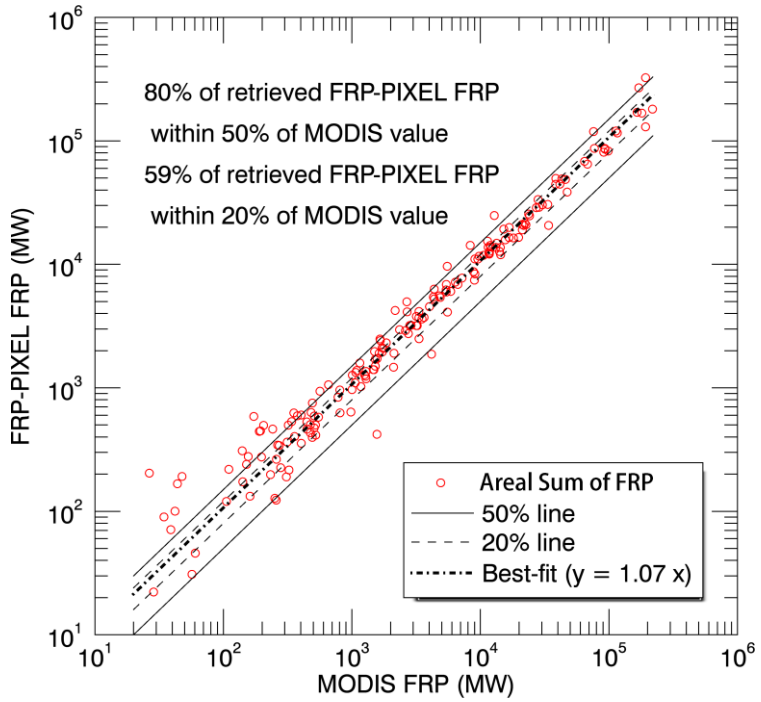

Figure 1. Relationship between regional-scale "Areal sum" of inter-scene FRP derived from all spatially matched, contemporaneous SEVIRI and MODIS in July 2015. Only the fires detected by both SEVIRI and MODIS are included in this regaional comparison.

3.2 FRP-GRID Product

Results from the FRP-GRID product evaluation are provided in Figure 13. The slope of the linear best fit to the FRP-GRID product and the MODIS-extracted matching 5° grid cell data (See Figure 7) lies close to unity, and the coefficient of variation (r^2) between the two datasets is 0.64. More than half of the FRP-GRID cells recording an hourly mean FRP in the FRP-GRID product were found to have an FRP within a factor of two of the value measured instantaneously by MODIS (Target Accuracy). A quarter were within 30% of the MODIS values.

Of course, the linear bias adjustments applied in the FRP-GRID product only capture the underlying macroscopic features of the sensor-to-sensor relationships, and do not

account for any temporal variability in the SEVIRI-to-MODIS ratios of FRP induced by diurnal or seasonal fluctuations in fire activity (e.g. as seen in Freeborn *et al.*, 2009). Nor can they deal well with situations where MODIS detects fire activity in a grid cell whilst SEVIRI does not, and so the linear bias corrections remain inactive. Nevertheless, by deriving different regression coefficients for each of the four LSA SAF regions, the FRP-GRID algorithm does account for broad spatial differences in the sensor-to-sensor relationships that potentially arise from (i) differences in fire regimes, and (ii) differences in SEVIRI view zenith angles, as explained in the FRP Product User Manual (PUM).

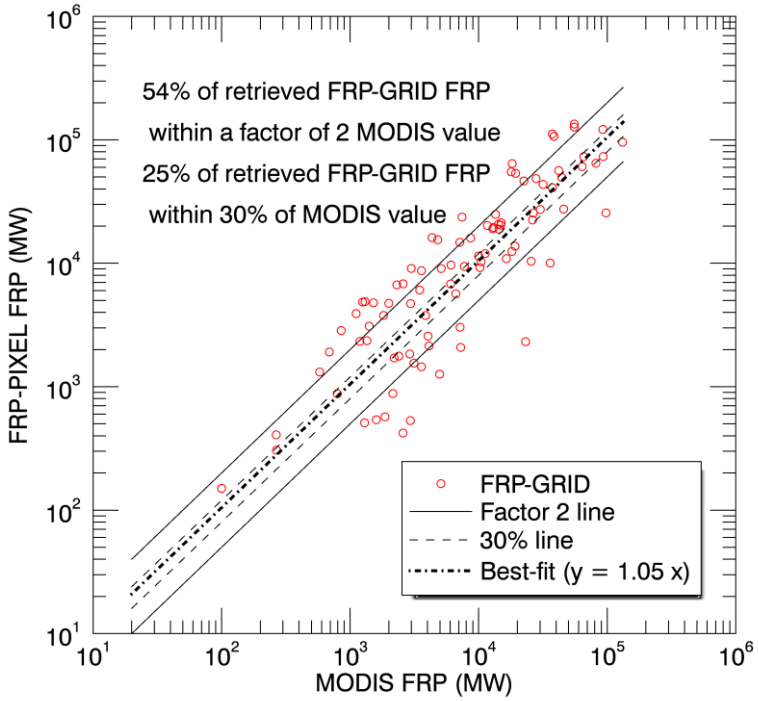

Figure 13. Evaluation of the bias adjustment factors used in the FRP-GRID product. Results are based on coincident SEVIRI and MODIS observations taken between in July 2015, collected and matched as shown in Figure 7. The near unity slope of the linear best fit between the FRP-GRID

and MODIS FRP derived data demonstrates the unbiased nature of the adjustment factors applied in the FRP-GRID product, in this case for 5.0° grid cells in southern Africa. The linear relationship representing a factor of 2 (Target accuracy), as well as one representing a 30% difference, are shown as solid and dashed lines respectively.

4. Conclusions

This evaluation has provided a detailed performance evaluation of the Metetosat SEVIRI FRP-PIXEL product, and also the summary FRP-GRID product, generated and disseminated by the EUMETSAT LSA SAF. On a per-fire basis there is a strong correlation (r^2 =0.74) between the FRP measures recorded in the geostationary FRP-PIXEL product and by the polar orbiting MODIS sensor near simultaneosuly, and a slope of the linear best fit line is close to unity (0.97). Overall, 79% of the SEVIRI-to-MODIS matchups have an FRP difference of less than 50%, and 62% of them less than 30%. It has shown that the SEVIRI FRP product therefore more than meets the Target Accuracy requirement.

We show that the FTA algorithm used in the SEVIRI FRP products appears more sensetive to fire than is the fire detection algorithm used within the MODIS active fire products (Collection 5), though SEVIRI is hampered in its detection of smaller fires by the relatively coarse size of the SEVIRI pixels (around an order of magnitude larger than the MODIS pixels at nadir). Nevertheless, calculations using the minimum confidently detectable FRP from SEVIRI indicate that the FTA algorithm detects actively burning fires covering down to around 1/10000th of a SEVIRI pixel (Wooster *et al.*, 2015). We show that fires with an FRP of less than 30 MW are more difficult to detect with SEVIRI than are fires above this threshold because of the instruments coarse pixel size, resulting in an FRP-PIXEL Active Fire Detection ommission error of 71% when assessed over the full Meteosat disk in July 2015 with respect to MODIS. The corresponding full disk FRP-PIXEL Active Fire detection commission Error is 13% with respect to MODIS, which is close to the typical values found in most active fire products (Roberts *et al.*, 2015).

In terms of the FRP-GRID product, which is in part designed to deal with the regional-scale FRP underestimation induced by the aforementioned active fire errors of omission, there is no directly comarable product available from MODIS (hourly average FRP within a 5° grid cell) with which to compare the FRP-GRID datasets. Nevertheless, using MODIS to make an esimate of the same value we find that more than half of the FRP-GRID cells recording an hourly mean FRP in the FRP-GRID product were found to have an FRP within a factor of two of the value measured instantaneously by MODIS (again meeting the products Target Accuracy).

Despite their coarse spatial resolution limitations for the detection of low FRP fires, the high temporal resolution provided from geostationary orbit offers an unprecedented high temporal resolution and is thus considered an important contributor to our ability to characterise fire emissions. As an example the reader is referred to Baldassarre *et al.* (2015) and Roberts *et al.* (2015) who provide examples of the use of the SEVIRI FRP-PIXEL product in characterising fire emisisons during a large fire event in Turkey and Greece respectively, and the resulting smoke emissions measures are there used to study the wildfire plume transport.

References:

EUMETSAT (2009). Fire Radiative Power Product User Manual. Technical Report SAF/LAND/IM/PUM FRP/1.1, EUMETSAT.

Freeborn, P.H., Wooster, M.J., Roberts, G., & Xu, W.D. (2014a). Evaluating the SEVIRI Fire Thermal Anomaly Detection Algorithm across the Central African Republic Using the MODIS Active Fire Product. *Remote Sensing*, *6*, 1890-1917

Freeborn, P.H., Wooster, M.J., Roberts, G., Malamud, B.D., & Xu, W.D. (2009). Development of a virtual active fire product for Africa through a synthesis of geostationary and polar orbiting satellite data. *Remote Sensing of Environment*, *113*, 1700-1711

Freeborn, P.H., Wooster, M.J., Roy, D.P., & Cochrane, M.A. (2014b). Quantification of MODIS fire radiative power (FRP) measurement uncertainty for use in satellite- based active fire characterization and biomass burning estimation. *Geophysical Research Letters*, *41*, 1988-1994

Giglio, L., Descloitres, J., Justice, C.O., & Kaufman, Y.J. (2003). An enhanced contextual fire detection algorithm for MODIS. *Remote Sensing of Environment*, *87*, 273-282

Giglio, L., van der Werf, G.R., Randerson, J.T., Collatz, G.J., & Kasibhatla, P. (2006). Global estimation of burned area using MODIS active fire observations. *Atmospheric Chemistry and Physics*, *6*, 957-974

Govaerts, Y., Wooster, M.J., Lattanzio, A. and Roberts. G. (2007), Fire Radiative Power (FRP) characterisation Algorithm Theoretical Basis Document, EUMETSAT, EUM/MET/SPE/06/0398

Guenther, A., Karl, T., Harley, P., Wiedinmyer, C., Palmer, P.I., & Geron, C. (2006). Estimates of global terrestrial isoprene emissions using MEGAN (Model of

Emissions of Gases and Aerosols from Nature). *Atmospheric Chemistry and Physics*, *6*, 3181-3210

Hyer, E.J., Reid, J.S., Prins, E.M., Hoffman, J.P., Schmidt, C.C., Miettinen, J.I., & Giglio, L. (2013). Patterns of fire activity over Indonesia and Malaysia from polar and geostationary satellite observations. *Atmospheric Research*, *122*, 504-519

Ichoku, C., Kaufman, Y.J., Giglio, L., Li, Z., Fraser, R.H., Jin, J.Z., & Park, W.M. (2003). Comparative analysis of daytime fire detection algorithms using AVHRR data for the 1995 fire season in Canada: perspective for MODIS. *International Journal of Remote Sensing*, *24*, 1669-1690

Ichoku, C., Martins, J.V., Kaufman, Y.J., Wooster, M.J., Freeborn, P.H., Hao, W.M., Baker, S., Ryan, C.A., & Nordgren, B.L. (2008). Laboratory investigation of fire radiative energy and smoke aerosol emissions. *Journal of Geophysical Research-Atmospheres*, *113*

Kaiser, J.W., Heil, A., Andreae, M.O., Benedetti, A., Chubarova, N., Jones, L., Morcrette, J.J., Razinger, M., Schultz, M.G., Suttie, M., & van der Werf, G.R. (2012). Biomass burning emissions estimated with a global fire assimilation system based on observed fire radiative power. *Biogeosciences*, *9*, 527-554

Kaufman, Y.J., Justice, C.O., Flynn, L.P., Kendall, J.D., Prins, E.M., Giglio, L., Ward, D.E., Menzel, W.P., & Setzer, A.W. (1998). Potential global fire monitoring from EOS-MODIS. *Journal of Geophysical Research-Atmospheres*, *103*, 32215-32238

Libonati, R., DaCamara, C.C., Pereira, J.M.C., & Peres, L.F. (2010). Retrieving middle-infrared reflectance for burned area mapping in tropical environments using MODIS. *Remote Sensing of Environment*, *114*, 831-843

Mayaux, P., Bartholome, E., Fritz, S., & Belward, A. (2004). A new land-cover map of Africa for the year 2000. *Journal of Biogeography*, *31*, 861-877

Reid, J.S., Hyer, E.J., Prins, E.M., Westphal, D.L., Zhang, J.L., Wang, J., Christopher, S.A., Curtis, C.A., Schmidt, C.C., Eleuterio, D.P., Richardson, K.A., & Hoffman, J.P. (2009). Global Monitoring and Forecasting of Biomass-Burning Smoke: Description of and Lessons From the Fire Locating and Modeling of Burning Emissions (FLAMBE) Program. *Ieee Journal of Selected Topics in Applied Earth Observations and Remote Sensing*, *2*, 144-162

Roberts, G., Wooster, M., Freeborn, P.H., & Xu, W. (2011). Integration of geostationary FRP and polar-orbiter burned area datasets for an enhanced biomass burning inventory. *Remote Sensing of Environment*, *115*, 2047-2061

Roberts, G., Wooster, M.J., & Lagoudakis, E. (2009a). Annual and diurnal african biomass burning temporal dynamics. *Biogeosciences*, *6*, 849-866

Roberts, G., Wooster, M.J., Lagoudakis, E., Freeborn, P., & Xu, W. (2009b). Continental Africa Biomass Burning Temporal Dynamics derived from MSG SEVIRI. *2009 Ieee International Geoscience and Remote Sensing Symposium, Vols 1-5*, 1458-1461

Roberts, G., Wooster, M.J., Perry, G.L.W., Drake, N., Rebelo, L.M., & Dipotso, F. (2005). Retrieval of biomass combustion rates and totals from fire radiative power observations: Application to southern Africa using geostationary SEVIRI imagery. *Journal of Geophysical Research-Atmospheres*, 110, 10.1029/2005JD006018

Roberts, G., Wooster, M. J., Xu, W., Freeborn, P. H., Morcrette, J.-J., Jones, L., Benedetti, A., Jiangping, H., Fisher, D., and Kaiser, J. W. (2015) LSA SAF Meteosat FRP products – Part 2: Evaluation and demonstration for use in the Copernicus Atmosphere Monitoring Service (CAMS), Atmos. Chem. Phys., 15, 13241-13267, doi:10.5194/acp-15-13241-2015

Roberts, G.J., & Wooster, M.J. (2008). Fire detection and fire characterization over Africa using Meteosat SEVIRI. *Ieee Transactions on Geoscience and Remote Sensing*, *46*, 1200-1218

Sofiev, M., Vankevich, R., Lotjonen, M., Prank, M., Petukhov, V., Ermakova, T., Koskinen, J., & Kukkonen, J. (2009). An operational system for the assimilation of the satellite information on wild-land fires for the needs of air quality modelling and forecasting. *Atmospheric Chemistry and Physics*, *9*, 6833-6847

van der Werf, G.R., Randerson, J.T., Giglio, L., Collatz, G.J., Kasibhatla, P.S., & Arellano, A.F. (2006). Interannual variability in global biomass burning emissions from 1997 to 2004. *Atmospheric Chemistry and Physics*, *6*, 3423-3441

van der Werf, G.R., Randerson, J.T., Giglio, L., Collatz, G.J., Mu, M., Kasibhatla, P.S., Morton, D.C., DeFries, R.S., Jin, Y., & van Leeuwen, T.T. (2010). Global fire emissions and the contribution of deforestation, savanna, forest, agricultural, and peat fires (1997-2009). *Atmospheric Chemistry and Physics*, *10*, 11707-11735

Wooster, M. J., Roberts, G., Freeborn, P. H., Xu, W., Govaerts, Y., Beeby, R., He, J., Lattanzio, A., Fisher, D., and Mullen, R. (2015). LSA SAF Meteosat FRP products – Part 1: Algorithms, product contents, and analysis. *Atmospheric Chemistry and Physics*, 15, 13217-13239, doi:10.5194/acp-15-13217-2015,

Wooster, M.J., Roberts, G., Perry, G.L.W., & Kaufman, Y.J. (2005). Retrieval of biomass combustion rates and totals from fire radiative power observations: FRP derivation and calibration relationships between biomass consumption

Formatada: EndNote Bibliography, Avanço: Esquerda: 0 cm, Pendente: 1.27 cm, Espaçamento entre linhas: Múltiplo 1.15 lin

Formatada: Tipo de letra: (predefinido) Times New Roman, 12 pt, Não Itálico

Formatada: Tipo de letra: (predefinido) Times New Roman, 12 pt, Cor do tipo de letra: Automática, Não verificar ortografia nem gramática, Padrão: Limpo

Formatada: Tipo de letra: (predefinido) Times New Roman, 12 pt, Não verificar ortografia nem gramática

Formatada: Não verificar ortografia nem gramática

Formatada: Tipo de letra: (predefinido) Times New Roman, 12 pt, Não verificar ortografia nem gramática

Formatada: Tipo de letra: (predefinido) Times New Roman, 12 pt, Cor do tipo de letra: Automática, Não verificar ortografia nem gramática, Padrão: Limpo

Formatada: Tipo de letra: (predefinido) Times New Roman, 12 pt, Não verificar ortografia nem gramática

and fire radiative energy release. *Journal of Geophysical Research-Atmospheres*, *110*, 10.1029/2005JD006318

Xu, W., Wooster, M.J., Roberts, G., & Freeborn, P. (2010). New GOES imager algorithms for cloud and active fire detection and fire radiative power assessment across North, South and Central America. *Remote Sensing of Environment*, *114*, 1876-1895

Zhukov, B., Lorenz, E., Oertel, D., Wooster, M., & Roberts, G. (2006). Spaceborne detection and characterization of fires during the bi-spectral infrared detection (BIRD) experimental small satellite mission (2001-2004). *Remote Sensing of Environment*, *100*, 29-51

EUMETSAT (2009). Fire Radiative Power Product User Manual. Technical Report SAF/LAND/IM/PUM FRP/1.1, EUMETSAT.

Freeborn, P.H., Wooster, M.J., Roberts, G., Malamud, B.D., & Xu, W.D. (2009). Development of a virtual active fire product for Africa through a synthesis of geostationary and polar orbiting satellite data. *Remote Sensing of Environment*, *113*, 1700-1711

Freeborn, P.H., Wooster, M.J., Roberts, G., & Xu, W.D. (2014a). Evaluating the SEVIRI Fire Thermal Anomaly Detection Algorithm across the Central African Republic Using the MODIS Active Fire Product. *Remote Sensing*, *6*, 1890-1917

Freeborn, P.H., Wooster, M.J., Roy, D.P., & Cochrane, M.A. (2014b). Quantification of MODIS fire radiative power (FRP) measurement uncertainty for use in satellite- based active fire characterization and biomass burning estimation. *Geophysical Research Letters*, *41*, 1988-1994

Giglio, L., Descloitres, J., Justice, C.O., & Kaufman, Y.J. (2003). An enhanced contextual fire detection algorithm for MODIS. *Remote Sensing of Environment*, *87*, 273-282

Giglio, L., van der Werf, G.R., Randerson, J.T., Collatz, G.J., & Kasibhatla, P. (2006). Global estimation of burned area using MODIS active fire observations. *Atmospheric Chemistry and Physics*, *6*, 957-974

Guenther, A., Karl, T., Harley, P., Wiedinmyer, C., Palmer, P.I., & Geron, C. (2006). Estimates of global terrestrial isoprene emissions using MEGAN (Model of Emissions of Gases and Aerosols from Nature). *Atmospheric Chemistry and Physics*, *6*, 3181-3210

Hyer, E.J., Reid, J.S., Prins, E.M., Hoffman, J.P., Schmidt, C.C., Miettinen, J.I., & Giglio, L. (2013). Patterns of fire activity over Indonesia and Malaysia from polar and geostationary satellite observations. *Atmospheric Research*, *122*, 504-519

Formatada: Tipo de letra: (predefinido) Times New Roman, 12 pt, Cor do tipo de letra: Automática, Não verificar ortografia nem gramática, Padrão: Limpo

Ichoku, C., Kaufman, Y.J., Giglio, L., Li, Z., Fraser, R.H., Jin, J.Z., & Park, W.M. (2003). Comparative analysis of daytime fire detection algorithms using AVHRR data for the 1995 fire season in Canada: perspective for MODIS. *International Journal of Remote Sensing, 24*, 1669-1690

Ichoku, C., Martins, J.V., Kaufman, Y.J., Wooster, M.J., Freeborn, P.H., Hao, W.M., Baker, S., Ryan, C.A., & Nordgren, B.L. (2008). Laboratory investigation of fire radiative energy and smoke aerosol emissions. *Journal of Geophysical Research-Atmospheres, 113*

Kaiser, J.W., Heil, A., Andreae, M.O., Benedetti, A., Chubarova, N., Jones, L., Morcrette, J.J., Razinger, M., Schultz, M.G., Suttie, M., & van der Werf, G.R. (2012). Biomass burning emissions estimated with a global fire assimilation system based on observed fire radiative power. *Biogeosciences, 9*, 527-554

Kaufman, Y.J., Justice, C.O., Flynn, L.P., Kendall, J.D., Prins, E.M., Giglio, L., Ward, D.E., Menzel, W.P., & Setzer, A.W. (1998). Potential global fire monitoring from EOS-MODIS. *Journal of Geophysical Research-Atmospheres, 103*, 32215-32238

Libonati, R., DaCamara, C.C., Pereira, J.M.C., & Peres, L.F. (2010). Retrieving middle-infrared reflectance for burned area mapping in tropical environments using MODIS. *Remote Sensing of Environment, 114*, 831-843

Mayaux, P., Bartholome, E., Fritz, S., & Belward, A. (2004). A new land-cover map of Africa for the year 2000. *Journal of Biogeography, 31*, 861-877

Reid, J.S., Hyer, E.J., Prins, E.M., Westphal, D.L., Zhang, J.L., Wang, J., Christopher, S.A., Curtis, C.A., Schmidt, C.C., Eleuterio, D.P., Richardson, K.A., & Hoffman, J.P. (2009). Global Monitoring and Forecasting of Biomass-Burning Smoke: Description of and Lessons From the Fire Locating and Modeling of Burning Emissions (FLAMBE) Program. *Ieee Journal of Selected Topics in Applied Earth Observations and Remote Sensing, 2*, 144-162

Roberts, G., Wooster, M., Freeborn, P.H., & Xu, W. (2011). Integration of geostationary FRP and polar-orbiter burned area datasets for an enhanced biomass burning inventory. *Remote Sensing of Environment, 115*, 2047-2061

Roberts, G., Wooster, M.J., & Lagoudakis, E. (2009a). Annual and diurnal african biomass burning temporal dynamics. *Biogeosciences, 6*, 849-866

Roberts, G., Wooster, M.J., Lagoudakis, E., Freeborn, P., & Xu, W. (2009b). Continental Africa Biomass Burning Temporal Dynamics derived from MSG SEVIRI. *2009 Ieee International Geoscience and Remote Sensing Symposium, Vols 1-5*, 1458-1461

Roberts, G., Wooster, M.J., Perry, G.L.W., Drake, N., Rebelo, L.M., & Dipotso, F. (2005). Retrieval of biomass combustion rates and totals from fire radiative

power observations: Application to southern Africa using geostationary SEVIRI imagery. *Journal of Geophysical Research-Atmospheres, 110*

Roberts, G., Wooster, M.J., Xu, W., Freeborn, P.H., Morcrette, J.J., Jones, L., Benedetti, A., & Kaiser, J. (2015). LSA SAF Meteosat FRP Products: Part 2 - Evaluation and demonstration of use in the Copernicus Atmosphere Monitoring Service (CAMS). *Atmos. Chem. Phys. Discuss., 15*, 15909-15976

Roberts, G.J., & Wooster, M.J. (2008). Fire detection and fire characterization over Africa using Meteosat SEVIRI. *Iece Transactions on Geoscience and Remote Sensing, 46*, 1200-1218

Sofiev, M., Vankevich, R., Lotjonen, M., Prank, M., Petukhov, V., Ermakova, T., Koskinen, J., & Kukkonen, J. (2009). An operational system for the assimilation of the satellite information on wild-land fires for the needs of air quality modelling and forecasting. *Atmospheric Chemistry and Physics, 9*, 6833-6847

van der Werf, G.R., Randerson, J.T., Giglio, L., Collatz, G.J., Kasibhatla, P.S., & Arellano, A.F. (2006). Interannual variability in global biomass burning emissions from 1997 to 2004. *Atmospheric Chemistry and Physics, 6*, 3423-3441

van der Werf, G.R., Randerson, J.T., Giglio, L., Collatz, G.J., Mu, M., Kasibhatla, P.S., Morton, D.C., DeFries, R.S., Jin, Y., & van Leeuwen, T.T. (2010). Global fire emissions and the contribution of deforestation, savanna, forest, agricultural, and peat fires (1997-2009). *Atmospheric Chemistry and Physics, 10*, 11707-11735

Wooster, M.J., Roberts, G., Freeborn, P.H., Xu, W., Govaerts, Y., Beeby, R., He, J., Lattanzio, A., & Mullen, R. (2015). Meteosat SEVIRI Fire Radiative Power (FRP) products from the Land Surface Analysis Satellite Applications Facility (LSA SAF) - Part 1: Algorithms, product contents and analysis. *Atmos. Chem. Phys. Discuss., 15*, 15831-15907

Wooster, M.J., Roberts, G., Perry, G.L.W., & Kaufman, Y.J. (2005). Retrieval of biomass combustion rates and totals from fire radiative power observations: FRP derivation and calibration relationships between biomass consumption and fire radiative energy release. *Journal of Geophysical Research-Atmospheres, 110*

Xu, W., Wooster, M.J., Roberts, G., & Freeborn, P. (2010). New GOES imager algorithms for cloud and active fire detection and fire radiative power assessment across North, South and Central America. *Remote Sensing of Environment, 114*, 1876-1895

Zhukov, B., Lorenz, E., Oertel, D., Wooster, M., & Roberts, G. (2006). Spaceborne detection and characterization of fires during the bi-spectral infrared detection

(BIRD) experimental small satellite mission (2001-2004). *Remote Sensing of Environment, 100*, 29-51

Govaerts, Y., Wooster, M.J., Lattanzio, A. and Roberts. G. (2007), Fire Radiative Power (FRP) characterisation Algorithm Theoretical Basis Document, EUMETSAT, EUM/MET/SPE/06/0398